Diver Relative AUV Navigation for Joint Human-Robot Operations

Andrew Streenan, LT USN and Noel E. Du Toit
Mechanical and Aerospace Engineering Department
Naval Postgraduate School, Monterey
Monterey, CA

***Abstract*— A novel application for Autonomous Underwater Vehicles (AUVs) is considered here: a robotic diver assistant that enables close-quarters robotic operations with human divers. A robotic diver assistant has the potential to improve the efficiency, effectiveness and safety of diver operations. The robot diver assistant must share the operating environment with human divers: the robot must navigate relative to the environment to reach a specified site location (along with moving divers), then maneuver among the mostly static divers as they perform their tasks on location. Strategies for navigating among divers while ensuring diver safety are presented in this paper. A reactive strategy, based on potential fields, is investigated with a deliberative approach that accounts for process and environmental disturbances, as well as measurement noise. The deliberative approach is based on the Partially Closed-Loop Receding Horizon Control method. Accounting for such uncertainties is required for close-quarter operations due to the challenges associated with underwater navigation and sensing.**

Keywords—Unmanned Underwater Vehicle; Tethered; Hovering; Autonomous Underwater Vehicle; Joint human-robot operations; dynamic, uncertain environments

I. BACKGROUND

Traditional Autonomous Underwater Vehicle (AUV) research has focused on long-range, open-ocean operations. However, a fundamentally different application domain has received little attention: close-quarters operations with human divers. The underwater domain is inherently dangerous to humans and diver operations are expensive due to limited diver bottom time and required surface support. To address some of these challenges, researchers at the Center for Autonomous Vehicle Research (CAVR) at the Naval Postgraduate School is developing a robotic diver assistant. A robotic diver assistant has the potential to improve the efficiency, effectiveness and safety of diver operations for all branches of professional divers (e.g., military, police, science, etc.). A core requirement for joint diver-robot operations is the ability to share the operational space with a human, which is investigated here. Of particular interest is the potential benefit to the Salvage, Explosive Ordinance Disposal (EOD), and Undersea Rescue operations of the Department of Navy.

Underwater operations are challenging due to communication and vehicle power constraints, as well as the sensory deprived nature of the underwater environment. However, one feature of the underwater domain that can be leveraged for joint human-robot operations is the slower environment dynamics: the divers' and robot's mobility is inherently constrained. These dynamic characteristics make this application domain attractive for the development of complex joint human-robot navigation algorithms since the decision cycle can be extended. On the other hand, accurate measurements of the underwater environment are difficult to obtain and large environmental disturbances exist. The robot has to operate in close proximity to the sea bottom (reefs, rocks, over-hangs, etc.) and divers and as a result it is critical to anticipate and account for the disturbances and uncertainties in the environment when solving the planning problem to ensure diver and robot safety.

Research related to close-quarter operations of AUVs and joint robot-diver operations is limited. The AQUA robot [1], [2] has been under development for a number of years, with a research emphasis on novel platform and propulsion design, as well as underwater computer vision techniques to sense and navigate the underwater domain. Specifically the robot uses a visual servo control to track and follow a human diver. The robot could then follow the same path on a future run. In contrast, this work focuses on control techniques to allow navigation among divers with a small, hovering class, tethered AUV. Also related is the development of the Hovering Autonomous Underwater Vehicle (HAUV) to perform hull inspections. This medium-sized (82 kg) vehicle uses a Doppler Velocity Log (DVL) and sonar to navigate relative to the hull of a ship [3], requires operation close to underwater objects, but is not concerned with joint human-robot operations.

Planning approaches based on reactive (e.g., potential field methods) and deliberative strategies (i.e., robotic motion planning approaches in dynamic, uncertain environment, DUE) as applicable to joint robot-diver operations are investigated here. Potential field methods is a reactive planning strategy that utilize attractive potentials to guide the robot towards some goal and repulsive potentials to avoid obstacles [4]. Potential field methods have been applied to establishing and maintaining formations of unmanned vehicles [5], avoiding obstacles [6], and changing the shape of the formation (e.g., [7]). These methods have also been applied to AUV obstacle avoidance [8]. A key benefit of these methods is the computational simplicity to implement various behaviors, but it is a purely reactive approach and does not predict the motion or activity of the diver.

Deliberative strategies are generally more difficult to implement in a dynamic uncertain environment, but the anticipative nature of the approaches lends itself to ensuring diver safety, particularly given the large environmental disturbances in the underwater domain. The future path of the

U.S. Government work not protected by U.S. copyright

This is a DRAFT. As such it may not be cited in other works. The citable Proceedings of the Conference will be published in IEEE Xplore shortly after the conclusion of the conference.

diver may not be known, but the range of motion of the diver can be predicted and assist in the motion planning process for the AUV. However, care must be taken when accounting for uncertainty since solutions tend to be conservative [9]. However, the Partially Closed Loop Receding Horizon Control (PCLRHC) approach [10] lends itself to the problem at hand since anticipated measurements are accounted for to limit this solution conservatism. The predictions can be improved if the goal of the diver is known to the AUV [11].

The focus of this research is the development of a planning and control strategy that allows *safe* joint robot-human diver operations for an AUV. An approach is desired that can simultaneously avoid the divers to ensure safety and follow the divers to provide mission assistance. The hardware and experimental setup is discussed in the following section. A simplified, decoupled model for the development AUV is presented, using an accurate off-board motion capture system, in Sec III. The potential field method is presented with simulation and experimental results in Sec. IV before a deliberative approach based on the PCLRHC approach is presented in Sec. V. Concluding remarks follow in Section VI.

II. Experimental Setup

A. Seabotix vLBV300

The experimental platform for this research is the SeaBotix vLBV300 platform, shown in Fig. 1 [12], is a tethered, Remotely Operated Vehicle (ROV). The vLBV300 has six thrusters, two for vertical and roll control, and four vectored thrusters for control in the surge, sway, and yaw directions, shown in Fig. 1. A computer control-interface has been developed for the vehicle that leverages a high-level (joystick) control interface (surge, sway, heave, yaw) and individual thruster control (surge, sway, heave, yaw, roll), resulting in a Tethered, Hovering Autonomous Underwater System (THAUS).

The vehicle coordinates are chosen to be positive x in the forward surge direction, positive y in the right sway direction, and positive z in the downward heave direction (refer to Fig. 2). Yaw is defined between $-\pi$ and $+\pi$ with zero in the positive x direction and increasing clockwise.

The platform currently has no onboard sensors (e.g, an inertial navigation system) and position and orientation measurements are obtained from an external system.

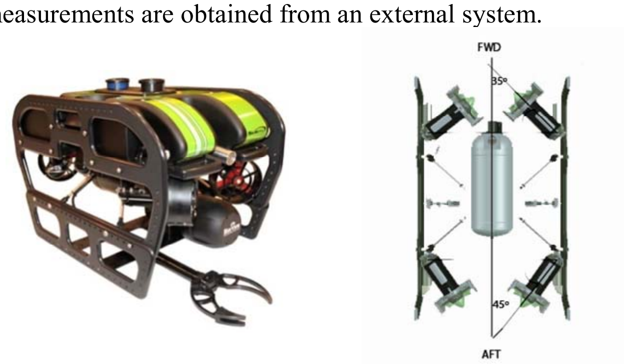

Fig. 1. The SeaBotix vLBV300 tethered AUV platform (*left*), and the planar vectored thruster configuration (*right*).

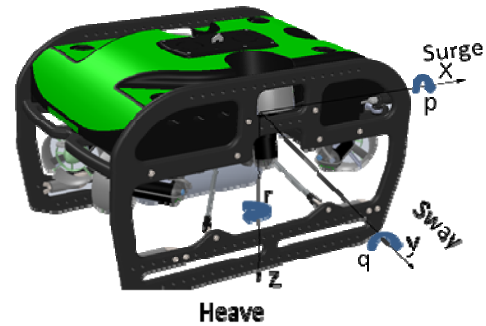

Fig. 2. THAUS body reference frame and variable definitions.

Fig. 3. NPS instrumented dive tank.

B. Vicon Motion Capture System

Position and orientation (pose) data for the vehicle are determined using a VICON motion capture (MoCap) system. The infrared (IR) camera-based MoCap system provides accurate marker tracking (<1cm) at a high rate (100 Hz). However, due to electro-magnetic wave attenuation in water, the current system can only be utilized above the water surface. THAUS has been extended with a low-inertia structure, which can be tracked by the MoCap system above the surface and from which the vehicle pose can be calculated. This structure does affect the vehicle dynamics, but these effects are neglected. Four infrared cameras surround the experimental test tank (see Fig. 3).

III. Decoupled Dynamic Models

A detailed, 6-DOF hydro-dynamic model of THAUS is currently being developed [13]. However, a simplified, decoupled dynamic model is desired for the motion of the vehicle in the surge, sway, and yaw directions for this work. First, the response of the system to high-level commands is investigated, before extending this model to allow position control. The models and associated assumptions are presented below.

A. Velocity Response

Utilizing the methods in [7], the decoupled planar dynamics of THAUS are determined by specifying a step input in the surge, sway, and yaw directions while recording the vehicle positions and velocities. The high-level (joystick) interface is used. It is assumed that the mapping between the joystick command and the resulting force is linear. Let $v(t)$ be the velocity and $f(t)$ be the force input (i.e., joystick command). In general, the transfer function for the plant is defined as (for surge, sway, and yaw):

$$P(s) = \frac{V(s)}{F(s)} \tag{1}$$

where *V(s)* and *F(s)* are the Laplace transforms of *v(t)* and *f(t)*, respectively (see Fig. 4). *f(t)* is a step input of magnitude K_j, resulting in:

$$F(s) = K_j \frac{1}{s}. \tag{2}$$

Fig. 4. Block diagram of the open-loop system (uncoupled), assuming a first-order system response.

Based on the response of the system in each individual channel (e.g., see Fig. 5 for the surge direction), a first-order model is assumed for the plant, written in terms of the steady state velocity (v_f) and time constant (t_c). The step response for a generic first order system is:

$$P_F(s) = \frac{K_p}{(s + \frac{1}{t_c})} \tag{3}$$

where $K_p = \frac{v_f}{K_j}$.

The results for the (assumed) uncoupled channels are presented in Table 1. As an example, the step input for the model is compared with the experimental results in the surge direction. This formulation implicitly assumes that the mapping between the joystick command magnitude (K_j) and the generated thruster force is linear. This is not the case, but since the objective is to develop simplified, decoupled dynamic models that will be used with feedback controllers, the resulting models are sufficient.

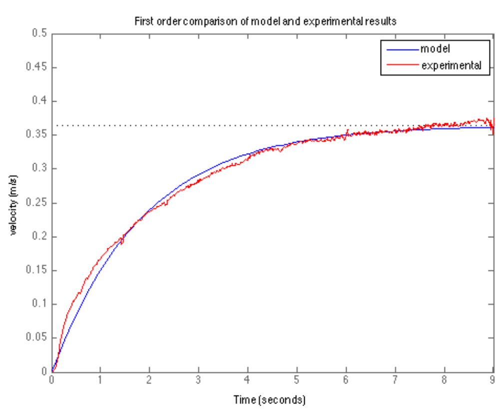

Fig. 5. Comparison of step responses from vehicle and model in the surge direction. Similar results were obtained for the sway and yaw channels.

TABLE I. FIRST ORDER TRANSFER FUNCTIONS DETERMINED FROM VELOCITY RESPONSE IN THE INDIVIDUAL CHANNELS

Channel	Transfer Function
Surge	$\frac{0.000622}{s+0.769}$
Sway	$\frac{0.000267}{s+0.667}$
Yaw	$\frac{0.0045}{s+2.5}$

B. Position Response

For the applications of interest, it is additionally desirable to control the position of the system. In order to develop a simple, uncoupled model, it is assumed that the required force is proportional to the position error between the reference and the actual vehicle position. This can be thought of as a crude potential field method (see Section IV).

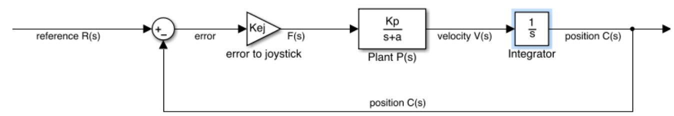

Fig. 6. Assumed position control block diagram, the closed-loop transfer function of which is a second order system.

A generic second order transfer function is given by:

$$G(s) = \frac{\omega_n^2}{s^2 + 2 \cdot \zeta \cdot \omega_n + \omega_n^2} \tag{4}$$

The values for percent overshoot and peak time can be used to completely define a second order system using:

$$\zeta = \frac{-\ln(\%OS/100)}{\sqrt{\pi^2 + \ln^2(\%OS/100)}}, \omega_n = \frac{\pi}{T_p\sqrt{1-\zeta^2}} \tag{5}$$

The values that are determined are for the second order response of the closed loop system. The open loop and closed loop system are related by

$$G_e(s) = \frac{G(s)}{1+G(s)} \tag{6}$$

where G(s) is the open loop transfer function. The open loop transfer function can then be calculated as:

$$G(s) = \frac{G_e(s)}{1-G_e(s)} \tag{7}$$

From the block diagram in Fig. 6:

$$G(s) = K_{ej} P(s) \frac{1}{s} \tag{8}$$

and therefore the plant is can be determined from the measured closed-loop response as:

$$P(s) = \frac{G(s)s}{K_{ej}} \tag{9}$$

where K_{ej} is the gain that scales the position error to force. Substituting the measured values for ζ and ω_V as well as the constant K_{ej}, the relationship for the plant is

$$P(s) = \frac{\omega_n^2 / K_{ej}}{s + 2\zeta\omega_n / K_{ej}} \tag{10}$$

Fig. 7 shows a comparison of a step response from the model determined by ζ and w_n to the actual response (for example in the surge direction). The model initially follows the vehicle response up to the maximum overshoot. The model and plant response then diverge due to the un-modeled nonlinearity in the joystick-force relationship. The settling time of both responses is about the same however, so this deviation is acceptable as the initial transient and final steady state values are the same. The resulting transfer functions for the plant based on this approach are given in Table 2.

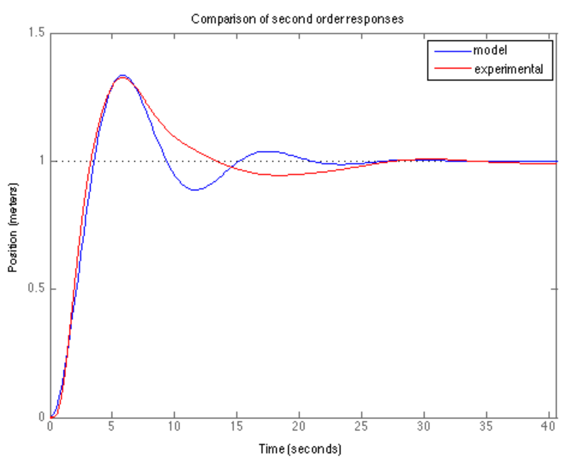

Fig. 7. Comparison of step responses from vehicle and model in the surge direction. Similar responses were obtained for the sway and yaw channels.

TABLE II. TRANSFER FUNCTIONS BASED ON POSITION RESPONSE OF THE SYSTEM IN THE INDIVIDUAL CHANNELS

Channel	Transfer Function
Surge	$\frac{0.000246}{s+0.238}$
Sway	$\frac{0.000126}{s+0.217}$
Yaw	$\frac{0.00381}{s+0.714}$

For station-keeping, it is desirable to force a position error to zero. Three separate proportional, integer, and derivative (PID) controllers were implemented for the surge, sway, and yaw channels. The station-keeping results in Fig. 8-10 show the response of the vehicle to several step commands as well as simulation results for the velocity and position models. These step commands were performed simultaneously for the three channels. Overall the position model and the plant response match. The step commands in the surge direction predict a higher percentage overshoot for the position model than the plant actually had. This is likely caused by the coupling occurring between the different channels by exciting the three directions at once. The position model is still desirable over the velocity model in surge because the second order dynamics (i,e,, overshoots and settling time) are similar to the plants. Table 3 contains the values for the PID controllers.

TABLE III. PID CONTROLLER DESIGN FOR STATION KEEPING

Channel	Proportional	Integral	Derivative
Surge	885	10	3175
Sway	1500	10	6000
Yaw	315	4	320

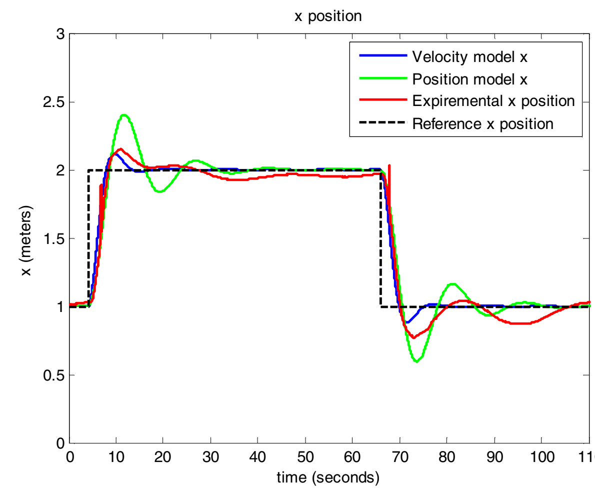

Fig. 8. Step responses in surge.

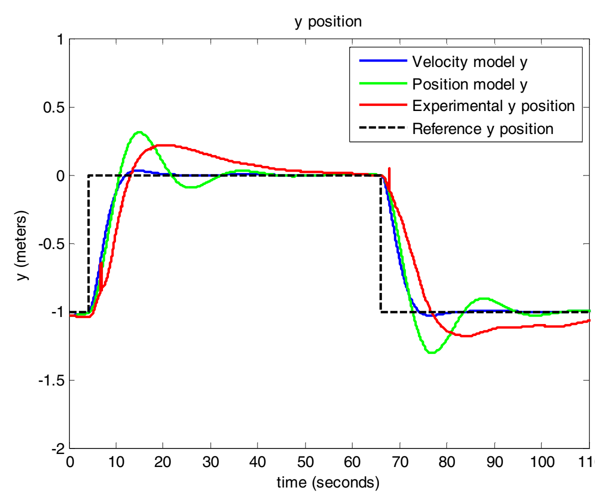

Fig. 9. Step responses in sway.

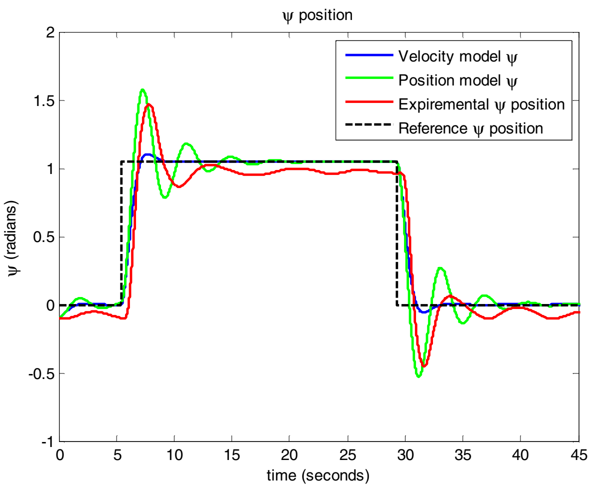

Fig. 10. Step responses in yaw

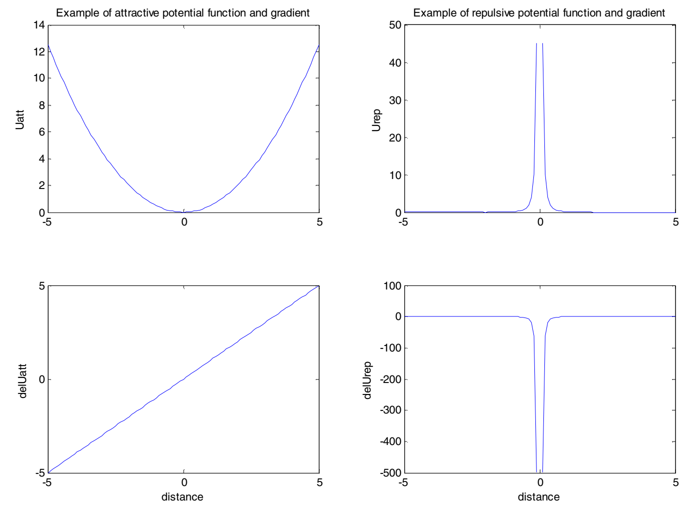

Fig. 11. Potential and gradient

IV. APPROACH: REACTIVE PLANNING

Potential field methods are attractive due to their computational efficiency and implementation simplicity. Various behaviors can be individually implemented as discrete potentials, the effects of which can then be super-imposed. A potential field consists of a sum of attractive (e.g., goal) and repulsive (e.g., diver) potentials (i.e., eq. (11)) to guide the vehicle from its current location to a goal. One drawback of the method is that the relative importance of these behaviors must be defined (by scaling the effects of the individual potentials). The negative of the gradient of the potential defines a force on the vehicle, which is assumed to be a particle. A virtual diver is created and the goal is specified relative to this diver's location: 1 meter to the diver's port side and pointing to a position 1 meter ahead of the diver (to simulate illuminating the diver's workspace).

$$U(q) = U_{att}(q) + U_{rep}(q) \tag{11}$$

1) Attractive Potential

The attractive potential given by [1] is used to pull the THAUS towards the goal location (refer to Fig. 11):

$$U_{att} = \frac{1}{2}\zeta d^2(q, q_{goal}) \tag{12}$$

whose gradient is

$$\nabla U_{att}(q) = \zeta(q - q_{goal}). \tag{13}$$

ζ is a three element proportional constant (scaling factor) used for each channel to achieve satisfactory response, q is the position of the ROV, and q_{goal} is the location of the goal.

2) Repulsive potential

To ensure diver safety, an aggressive repulsive potential is used to push the robot away from the diver (refer to Fig. 11):

$$\begin{aligned} &U_{rep}(q) = \frac{1}{2}\eta\left(\frac{1}{D(q)} - \frac{1}{Q^*}\right)^2, D(q) \le Q^* \\ &U_{rep}(q) = 0, D(q) > Q^* \end{aligned} \tag{14}$$

whose gradient is

$$\begin{aligned} &\nabla U_{rep}(q) = \eta\left(\frac{1}{Q^*} - \frac{1}{D(q)}\right)\frac{1}{D^2(q)}\nabla D(q), D(q) \le Q^*. \\ &\nabla U_{rep}(q) = 0, D(q) > Q^* \end{aligned} \tag{15}$$

D is the distance between the ROV and the diver and $Q^*=0.8$ meters is a threshold distance beyond which this behavior is ignored (i.e., the robot is far from the diver). As an additional measure of safety, at 0.5 meters from the diver the attractive potential is disabled. Fig. 12 shows a simulated run where the goal is on the opposite side of the diver from the ROV. The repulsive potential keeps the ROV away from the diver and the ROV is able to navigate around the diver to the goal. On the same figure, the measured path of THAUS navigating the same scenario and using the reactive scheme verifies the desired behavior.

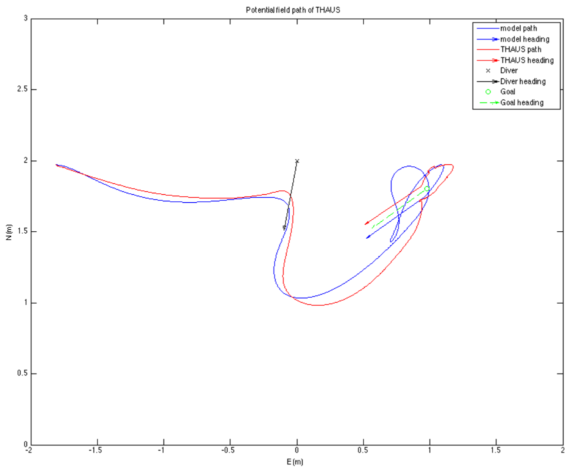

Fig. 12. Simulated (blue) and measured (red) paths using the potential field method.

3) *Performance Improvement*

A disadvantage to using the potential field is that it is purely reactive. As a result, the ROV will always lag behind the goal if the diver is moving. Two improvements are made to the attractive potential to speed up the response and minimize steady state error. To speed up the response of the diver, an additional attractive potential function is added to match vehicle velocity with diver velocity:

$$\nabla U_{vel}(V) = \zeta_v (V - V_{goal}) \tag{16}$$

V is the velocity of the ROV and V_{goal} is the velocity of the goal. This term is tuned to provide a rapid input to the vehicle as soon as the diver moves. The potential gradient $\nabla U_{\text{int}} = \zeta_{\text{int}} \int (q - q_{goal}) dt$ is added to drive steady state error in velocity to zero. This potential will increase over time if there is an error between the ROV and goal. This potential acts to drive that error to zero. Fig. 13 compares the position error between the robot and the specified goal with and without these additional behaviors. The figure shows that the improved approach has a quicker response, less peak error, and smaller steady state error than the potential field alone.

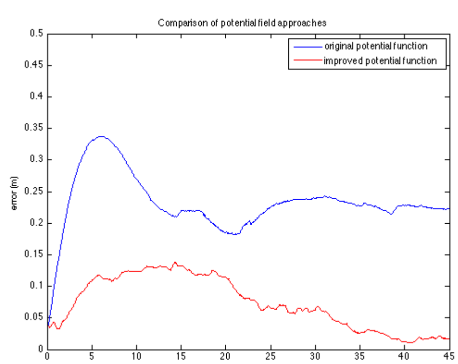

Fig. 13. Experimental comparison of the two potential field approaches

V. Approach: Deliberative Planning

Underwater robotic mission execution is challenging in part due to large environmental disturbances (e.g., surge and current), highly-coupled and non-linear motion models and communication limitations. The problem is exacerbated by measurement noise, relatively low resolution sensors, and the absence of a global position system. For these reasons, it is important to account for uncertainty in the robot's state (i.e., how well it knows its own location, speed, etc.) as well as the divers' uncertainty when sharing the workspace with humans. Furthermore, professional divers operate with purpose, either moving towards a goal location, or executing a task locally. For these reasons, it is necessary to deliberate over the divers' actions when planning appropriate motion in the workspace.

Planning approaches that account for stochastic uncertainty has mostly been applied to static environments (e.g., [14],[15]). Extensions of these approaches to dynamic, uncertain environments violate key assumptions, and alternative approaches base on Stochastic Dynamic Programming have been investigated (e.g., [16],[9]). In this work, the methods of [10] are applied to a dynamic model developed for the vLBV300 developed in [13] that has been specialized to planar motion. Chance constraint results from [17] are also leveraged to ensure safe motion among human divers.

A. *Planar Coupled Hydrodynamic Robot Model*

A detailed 6-DOF hydrodynamic model for the vLBV300 is presented in [13]. The vehicle can be commanded in the surge, sway, heave, yaw, and roll directions (see Section II). For the problem at hand, motion is constrained to a plane, resulting in zero dynamics in heave, pitch, and roll. According to Fig. 2, surge is in the *x*-direction, with surge velocity *u*. Sway is in the *y*-direction, with sway velocity *v*. Yaw, ψ, is a rotation around the z-axis, with an associated angular velocity *r*. Let $\eta = [x \quad y \quad \psi]^T$ and $\upsilon = [u \quad v \quad r]^T$ be the state vectors associated with pose and velocities, respectively, and $\tau = [X \quad Y \quad N]$ be the input vector, then the resulting equations of motion are:

$$\dot{\eta} = J(\eta)\upsilon + \omega_\eta \tag{17}$$

where

$$J(\eta) = \begin{bmatrix} \cos(\psi) & \sin(\psi) & 0 \\ -\sin(\psi) & \cos(\psi) & 0 \\ 0 & 0 & 1 \end{bmatrix} \tag{18}$$

and $\omega_\eta = \omega_\eta(t) \sim N(0, \mathrm{W}_\eta)$ is the process noise associated with the pose. The velocities in the body frame evolve according to:

$$\dot{\upsilon} = f_\upsilon(\upsilon, \eta, \tau) + \omega_\upsilon \tag{19}$$

where

$$f_\upsilon(\upsilon,\eta,\tau) = \begin{bmatrix} \dfrac{1}{(m-X_{\dot{u}})}\left((m-Y_{\dot{v}})vr - X_{u|u|}u|u| + X\right) \\ \dfrac{1}{(m-Y_{\dot{v}})}\left(-(m-X_{\dot{u}})ur + Y_{v|v|}v|v| + Y\right) \\ \dfrac{1}{(I_Z-N_{\dot{r}})}\left(-(X_{\dot{u}}-Y_{\dot{v}})uv + N_{r|r|}r|r| + N\right) \end{bmatrix}. \quad (20)$$

m is the vehicle in-air mass, I_z is the moment of inertia around the z-axis, $X_{\dot{u}}$, $Y_{\dot{v}}$, and $N_{\dot{r}}$ are coefficient associated with the hydrodynamic added mass, and $X_{u|u|}$, $Y_{v|v|}$, and $N_{r|r|}$ are coefficients associated with hydrodynamic damping [18]. X and Y are the commanded forces in the surge and sway directions, respectively, and N is the commanded moment in the yaw direction. These commands have been related to individual thruster commands in [13]. Finally, $\omega_\upsilon = \omega_\upsilon(t) \sim N(0, \mathrm{W}_\upsilon)$ is the disturbance, which is assumed to be Gaussian. Define the augmented system: $\mu = [\eta \quad \upsilon]^T$, $f(\mu,\tau) = [J(\eta) \quad f_\upsilon(\upsilon,\eta,\tau)]^T$ and $\omega = [\omega_\eta \quad \omega_\upsilon] \sim N(0,W)$, then the system dynamics are given by:

$$\dot{\mu} = f(\mu,\tau) + \omega \quad (21)$$

This system can readily be converted into a discrete-time system (e.g., using a numerical integration scheme and applying a constant control for the duration of the discrete time step) to yield:

$$\mu_i = f_d(\mu_{i-1}, \tau_{i-1}) + \omega_{i-1} \quad (22)$$

It is assumed that only η can be measured directly, resulting in a linear measurement model:

$$y_i = C\mu_i + \gamma_i \quad (23)$$

Where $C = [I_{3x3} \quad 0_{3x3}]$ and $\gamma_i \sim N(0,V)$ is Gaussian measurement noise.

The parameter values used in this work were obtained for the vLBV300 in [13] (summarized in Table IV). Furthermore, the covariance for the disturbances $W = \mathrm{diag}\left(\left[0.2^2, 0.2^2, 0.01^2, 0.1^2, 0.1^2, 0.01^2\right]\right)$ and measurement noise: $V = \mathrm{diag}\left(\left[0.2^2, 0.2^2, 0.05^2\right]\right)$.

TABLE IV. HOVERING-CLASS VECTORED ROV MODEL COEFFICIENTS

m [kg]	I_z [kg.m^2]	$X_{\dot{u}}$ [kg]	$Y_{\dot{v}}$ [kg]
20.9	0.90	-19.52	-17.06
$N_{\dot{r}}$ [kg.m^2/rad]	$X_{u\|u\|}$ [kg/m]	$Y_{v\|v\|}$ [kg/m]	$N_{r\|r\|}$ [kg.m^2/rad^2]
-0.906	-41.34	-7.33	-0.349

B. Diver Model

A simple linear discrete time model is assumed for the diver: the diver travels at constant velocity, but disturbances affect the diver trajectory. Other models, including traveling towards a goal location, will be considered in the future. The model is:

$$\begin{aligned} x_i^D &= A_D x_{i-1}^D + F_D \omega_{i-1}^D \\ y_i^D &= C_D x_i^D + \gamma_i^D \end{aligned} \quad (24)$$

where

$$A_D = \begin{bmatrix} 1 & 0 & \Delta t & 0 \\ 0 & 1 & 0 & \Delta t \\ 0 & 0 & 1 & 0 \\ 0 & 0 & 0 & 1 \end{bmatrix} \qquad \begin{aligned} F_D &= [0_{2\times2} \quad I_{2\times2}]^T \\ C_D &= [I_{2\times2} \quad 0_{2\times2}] \end{aligned} \quad (25)$$

and $\omega_i^D \sim N(0,W_D)$ and $\gamma_i^D \sim N(0,V_D)$. In this work, the covariance for the disturbances $W_D = \mathrm{diag}\left(\left[0.1^2, 0.1^2\right]\right)$ and measurement noise: $V_D = \mathrm{diag}\left(\left[0.1^2, 0.1^2\right]\right)$ were assumed.

C. Stochastic Receding Horizon Control

The Stochastic Receding Horizon Control formulation [10] can be applied to the above non-linear hydro-dynamic model. This approach recursively re-solves the stochastic non-linear, constrained optimization problem over a specified horizon at each time step. It is convenient to convert the problem into the *discrete space* (e.g., using a numerical optimization technique) and to re-write the system dynamics (i.e., (21) and (23)) in terms of the *belief state*, such that the belief at state i is:

$$b_i = p(\mu_i \mid \tau_{0:i-1}, y_{0:i}) \quad (26)$$

$\tau_{0:i}$ is the sequence of control inputs and $y_{0:i}$ is the sequence of measurements obtained up to stage i. This belief state can be recursively calculated from the previous value via Bayes Rule. For example, for a linear system with Gaussian noise, this belief state update is given by the Kalman Filter. Let $b_i = f_b(b_{i-1}, \tau_{i-1}, y_i)$ be this update, then the optimization problem of interest can be written as [10]:

$$\begin{aligned} \min_{\tau_{k:m}} \quad & \mathrm{E}\left[c_m(b_m) + \sum_{i=1}^{m-1} c_i(b_i, \tau_i)\right] \\ \text{s.t.} \quad & b_i = f_b(b_{i-1}, \tau_{i-1}, y_i) \\ & \mathrm{P}\left(g_b(b_i, \tau_i) \le 0\right) \ge \beta \end{aligned} \quad (27)$$

where c_i are the cost terms of the additive objective function and m is the planning horizon. In order to solve the planning problem, it is necessary to make some assumptions about the anticipated information that the robot will gain during plan execution. Two strategies are investigated below: ignoring all future measurements (resulting in the Open-Loop Receding Horizon Control, or OLRHC, approach) and assuming that the most likely measurement will occur (resulting in the Partially Closed-Loop Receding Horizon Control, or PCLRHC, approach).

It is important to note that due to the uncertain states, the constraints must be formulated as chance constraints [17]. It is shown that linear constraints of the form $\alpha^T \mu \leq \chi$ with $\mu \sim N(\hat{\mu}, \Sigma)$ can be written as a chance constraint $P\left(\alpha^T \mu \leq \chi\right) \geq \beta$ in terms of the state distribution parameters (i.e., belief state) as:

$$\alpha^T \hat{\mu} \leq \chi - F^{-1}(\beta) \times \sqrt{\alpha^T \Sigma \alpha} \quad (28)$$

where $F^{-1}(\beta)$ is the inverse of the cumulative distribution function for a standard scalar Gaussian (can be obtained from a lookup table). Thus, the chance constraint on an uncertain state is re-written in term of the distribution parameters of that state. The effect of the state uncertainty is to back-off from the constraint. $\beta = 0.99$ is assumed for the linear constraints.

In a similar way, collision constraints between two objects with position uncertainty can be enforced: $P(\text{Coll}) \leq \beta$. If the objects are circular and the states have Gaussian distributions then collision constraints can be enforced using a quadratic function [17]. Let μ_1 be the position state vector for object 1 with an assumed distribution: $\mu_1 \sim N\left(\hat{\mu}_1, \Sigma_1\right)$, and similarly for object 2, then, the collision chance constraint is approximately satisfied when:

$$\left(\hat{\mu}_1 - \hat{\mu}_2\right)^T \Sigma_C^{-1} \left(\hat{\mu}_1 - \hat{\mu}_2\right) \leq \kappa \quad (29)$$

where $\Sigma_C = \Sigma_1 + \Sigma_2$. κ is a function of the level of certainty for constraint violation, β , the object geometries, and combined distribution shape, Σ_C. Du Toit and Burdick [17] developed a look-up table for two circular objects to ensure collision constraint satisfaction, which is used here. $\beta = 0.01$ is assumed for the collision chance constraints.

D. Open-Loop Receding Horizon Control (OLRHC)

Let k denote the current stage (time). According to OLRHC, all future measurements are ignored. Thus, the belief state at some future stage $i>k$ is given by:

$$b_i^{OL} = p(\mu_i \mid \tau_{0:k-1}, \tau_{k:i-1}, y_{0:k}) \quad (30)$$

Practically, the uncertainty associated with the system state continues to grow (according to the dynamics and disturbance model). The recursive update of the belief state for the system defined in (22) and (23) is obtained with the Extended Kalman Filter (EKF). Eq. (22) must be linearized to apply the Kalman Filter machinery. However, since measurements beyond the current stage k are ignored, only the prediction step of the Extended Kalman Filter is performed:

$$\begin{aligned} \hat{\mu}_{i|i-1} &= f_d(\hat{\mu}_{i-1|i-1}, \tau_{i-1}) \\ \Sigma_{i|i-1} &= A_{i-1}\Sigma_{i-1|i-1} + \Sigma_{i-1|i-1}A_{i-1}^T + W_{i-1} \\ \hat{\mu}_{i|i} &= \hat{\mu}_{i|i-1} \qquad \Sigma_{i|i} = \Sigma_{i|i-1} \end{aligned} \quad (31)$$

where $A_{i-1} \triangleq \left.\frac{\partial f}{\partial \mu}\right|_{\hat{\mu}_{i-1|i-1}, \tau_{i-1}}$. The same steps are performed for the diver, and these open-loop belief states are used to evaluate the cost function as well as chance constraints.

The solutions associated with the OLRHC approach tend to be conservative since all anticipated information is ignored. This can be seen in Fig. 14 where a diver is assumed to travel at constant velocity and the robot predicts the diver location 5s into the future and then plans to move into position next to the diver, but offset by 2m to the diver's right.

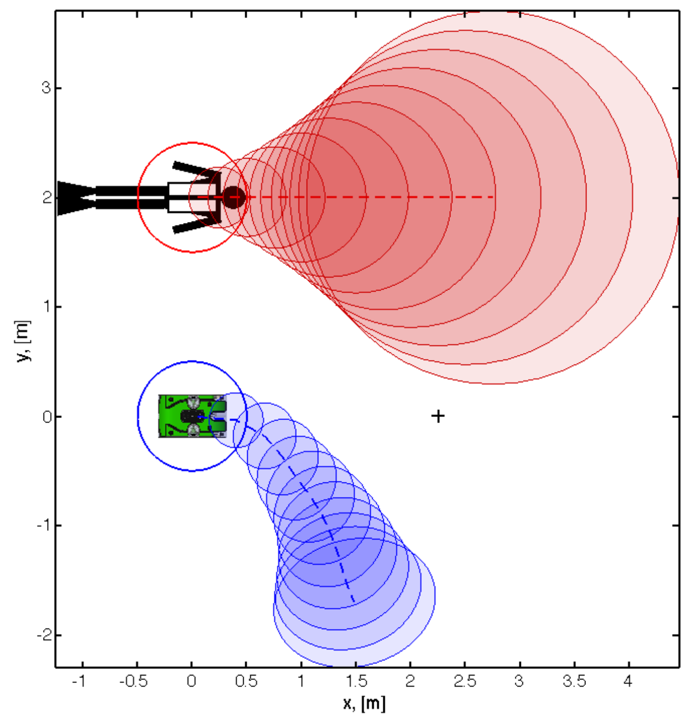

Fig. 14. The predicted belief states of the diver and the resulting motion plan for the robot that satisfies the chance constraints for the OLRHC approach.

Due to the growth in the uncertainty in the position states of the diver and robot (red and blue ellipses, respectively), the planned path moves the robot away from the goal location in order to satisfy the chance constraints. The effective objects used to enforce the collision constraints have a radius of 0.5m and are indicated by the blue and red circles for the robot and diver, respectively.

E. Partially Closed-Loop RHC (PCLRHC)

Unlike the OLRHC approach, the PCLRHC approach assumes that the most likely measurement will occur in the future. Thus, the belief state can be written as:

$$b_i^{PCL} = p(\mu_i \mid \tau_{0:k-1}, \tau_{k:i-1}, y_{0:k}, \tilde{y}_{k+1:i}) \quad (32)$$

where $\tilde{y}_i$ is the most likely measurement. As for the OLRHC approach, the EKF prediction step is performed as in eq. (31). However, this belief state is further updated to reflect the anticipated measurement. The effect of the measurement is to both updates the shape of the distribution in a predictable manner and the value of the measurement shifts the mean. The former step can be performed without knowing the value of the measurement. The latter step is ignored since it was shown in [10] that any assumed measurement other than the most likely measurement will result in an artificial reduction in entropy (which is not desirable). The update steps are given by:

$$\begin{aligned} \hat{\mu}_{i|i} &= \hat{\mu}_{i|i-1} \\ \Sigma_{i|i} &= \left(I - K_i C_i\right)\Sigma_{i|i-1} \end{aligned} \tag{33}$$

where $K_i = \Sigma_{i|i-1} C_i^T \left(C_i \Sigma_{i|i-1} C_i^T + V_i\right)^{-1}$. Note that the mean of the distribution is not updated.

The planned path from the PCLRHC approach is plotted in Fig. 15. The uncertainty growth is limited since anticipated measurements are taken into account, and the solution is significantly less conservative while still accounting for the uncertainty. However, it is important to realize that the problem must be recursively re-solved to account for the actual measurements since these measurements will affect the actual belief states during motion execution.

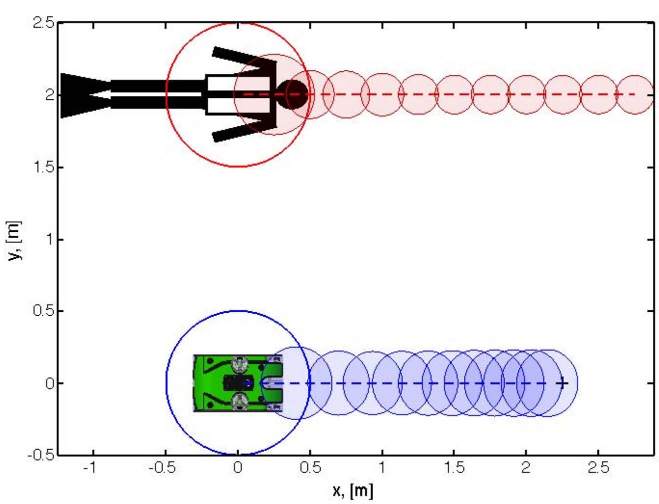

Fig. 15. The predicted belief states of the diver and the resulting motion plan for the robot that satisfies the chance constraints for the PCLRHC approach.

Since the conservatism associated with motion planning in the dynamic, uncertain environment is overcome by accounting for the anticipated information during plan execution, this deliberative approach is particularly suitable for joint diver-robot operations.

VI. CONCLUSION

Closed-quarters operations with AUVs allows for the exploration of novel applications, including joint diver-robot operations. However, diver safety is of paramount importance when the human and robot must share a workspace. Reactive and deliberative methods were investigated in this work. A simplified, decoupled dynamic model for a hovering-class AUV is developed for the SeaBotix vLBV300 platform. This model is used to develop reactive diver avoidance and robot positioning in simulation. The potential field method is utilized for this purpose and shows satisfactory results for a static diver. This approach was implemented on the platform and experimental results are presented. The method was extended to handle the case where the diver is moving by incorporating additional behaviors that also track the diver velocity. Simulation results indicate a significant improvement in diver-relative motion tracking. The key advantage of the reactive approach is computational efficiency. However, it is recognized that deliberative planning may be required for diver-relative navigation in complex scenarios (e.g., moving around structures in the presence of surge). To this end, a deliberative approach that accounts for diver motion and robot, diver, and environmental uncertainties. The approach is based on the Partially Closed-Loop Receding Horizon Control approach. Using a coupled, 3-DOF motion model of the vLBV300, simulation results highlight the challenges associated with deliberative motion in the presence of uncertainty (e.g., computational complexity, conservatism, etc.) while verifying the applicability of the approach to the problem of diver-relative navigation.

REFERENCES

[1] C. Georgiades, A. German, A. Hogue, H. Liu, C. Prahacs, A. Ripsman, R. Sim, L. Torres, P. Zhang and M. Buehler, "AQUA: An aquatic walking robot," in *Intelligent Robots and Systems, 2004.(IROS 2004). Proceedings. 2004 IEEE/RSJ International Conference On,* 2004, pp. 3525-3531.

[2] G. Dudek, M. Jenkin, C. Prahacs, A. Hogue, J. Sattar, P. Giguere, A. German, H. Liu, S. Saunderson and A. Ripsman, "A visually guided swimming robot," in *Intelligent Robots and Systems, 2005.(IROS 2005). 2005 IEEE/RSJ International Conference On,* 2005, pp. 3604-3609.

[3] J. Vaganay, M. Elkins, D. Esposito, W. O'Halloran, F. Hover and M. Kokko, "Ship hull inspection with the HAUV: US navy and NATO demonstrations results," in *OCEANS 2006,* 2006, pp. 1-6.

[4] H. M. Choset, *Principles of Robot Motion: Theory, Algorithms, and Implementation.* Bradford Books, 2005.

[5] L. Barnes, M. Fields and K. Valavanis, "Unmanned ground vehicle swarm formation control using potential fields," in *Control & Automation, 2007. MED'07. Mediterranean Conference On,* 2007, pp. 1-8.

[6] O. Khatib, "Real-time obstacle avoidance for manipulators and mobile robots," *The International Journal of Robotics Research,* vol. 5, pp. 90-98, 1986.

[7] F. E. Schneider and D. Wildermuth, "A potential field based approach to multi robot formation navigation," in *Robotics, Intelligent Systems and Signal Processing, 2003. Proceedings. 2003 IEEE International Conference On,* 2003, pp. 680-685.

[8] M. Porfiri, D. G. Roberson and D. J. Stilwell, "Tracking and formation control of multiple autonomous agents: A two-level consensus approach," *Automatica,* vol. 43, pp. 1318-1328, 8, 2007.

[9] J. Yan and R. R. Bitmead, "Incorporating state estimation into model predictive control and its application to network traffic control," *Automatica,* vol. 41, pp. 595-604, 2005.

[10] N. E. Du Toit and J. W. Burdick, "Robot motion planning in dynamic, uncertain environments," *Robotics, IEEE Transactions On,* vol. 28, pp. 101-115, 2012.

[11] S. Thompson, T. Horiuchi and S. Kagami, "A probabilistic model of human motion and navigation intent for mobile robot path planning," in

Autonomous Robots and Agents, 2009. ICARA 2009. 4th International Conference On, 2009, pp. 663-668.

[12] *vLBV Operators Manual*, D rev., SeaBotix., San Diego, CA, 2011, pp. 9-10

[13] J. Weiss and N. Du Toit, "Real-time dynamic model learning and adaptation for underwater vehicles," unpublished .

[14] S. Prentice and N. Roy, "The belief roadmap: Efficient planning in belief space by factoring the covariance," *The International Journal of Robotics Research,* vol. 28, pp. 1448-1465, 2009.

[15] R. Alterovitz, T. Siméon and K. Y. Goldberg, "The stochastic motion roadmap: A sampling framework for planning with markov motion uncertainty." in *Robotics: Science and Systems,* 2007, pp. 246-253.

[16] D. P. Bertsekas, *Dynamic Programming and Optimal Control.* MA: Athena Scientific, 2005.

[17] N. E. Du Toit and J. W. Burdick, "Probabilistic collision checking with chance constraints," *Robotics, IEEE Transactions On,* vol. 27, pp. 809-815, 2011.

[18] T. I. Fossen, "Guidance and control of ocean vehicles," *New York,* 1994.